# Physics-informed machine learning for wind turbulence reconstruction with lidar under aircraft motion


Amaury Capmas-Pernet — *DOTA, ONERA, Université Paris-Saclay, 91120, Palaiseau, France*
Christian Musso — *DOTA, ONERA, Université Paris-Saclay, 91120, Palaiseau, France*
Frédéric Dambreville — *DOTA, ONERA, Université Paris-Saclay, 91120, Palaiseau, France*
Tomline Michel — *DOTA, ONERA, Université Paris-Saclay, 91120, Palaiseau, France*



## Abstract

We propose a physics-informed machine learning method for reconstructing 3d turbulent wind from partial, noisy and accumulated over time observations obtained via lidar measurements. This method, which is optimal in terms of mean squared error, combines Gaussian process regression with a physics-informed kernel that leverages prior knowledge of the turbulence structure, as provided by the von Karman turbulence model. The proposed method allows for the incorporation of observations accumulated during the aircraft's motion. Furthermore, we demonstrate its robustness when turbulence parameters must be estimated.



Proceedings of the 2nd International Conference on Probabilistic Numerics (ProbNum) 2026, Lappeenranta, Finland. PMLR Volume 341.



## 1 Introduction

One of the most promising ways to reduce the environmental impact of future aircraft is to reduce their drag by equipping them with very high aspect ratio wings. Unfortunately, due to their size, these wings will be subjected to much greater load stresses, particularly those caused by turbulence. As these loads could endanger the structural integrity of the aircraft, one possibility is to reinforce the wings with additional metal frame but in this case the added weight would reduce the energy gain. Another option is to use adaptive wings whose aerodynamic profile changes in response to turbulent wind upstream of the aircraft. This method requires an accurate determination of the three-dimensional (3d) wind upstream of the aircraft. Wind measurement is typically performed with a direct detection molecular lidar located at the front of the airplane in order to detect wind early enough to allow the wings to adjust. These measurements are taken at points in space along specific directions from the aircraft, known as lidar axes. However, these measurements are only partial observations, that is, the projection of turbulent wind onto the lidar axes. Furthermore, errors can occur during the measurement process, this is referred to as measurement noise. Nevertheless, starting from these partial and noisy observations, we aim to reconstruct the 3d wind at any point in space.

Reconstruction methods have been developed for turbulences (Fezans et al., 2019; Krishnamurthy, 2023) and for gusts (Musso et al., 2024). Here we generalize a method developed in Capmas-Pernet et al. (2026) which combines, in a static setting, Gaussian process regression with a turbulence model known as the Von Karman model. Here we extend this work to define a procedure for estimating the parameters of the Von Karman model via maximum likelihood estimation. Furthermore, we develop a reconstruction method that takes into account the observations accumulated during the aircraft's flight. This method improves the reconstruction by taking advantage of the underlying physics of turbulence. To do this, we will use von Karman's model (von Kármán, 1948) for homogeneous and isotropic turbulence as our physical model. Unlike other classical models, such as the Navier-Stokes equations, this model is stochastic in the sense that it provides the covariance matrix between the wind velocity vectors at two points in space. Because of this characteristic, we will incorporate it into a machine learning method belonging to the class of kernel methods. Furthermore, since this model incorporates the a priori knowledge of the turbulence structure we can describe it as a "physics-informed kernel". The method we will use is Gaussian process regression (or kriging, Krige, 1951) that minimizes the mean square reconstruction error given our partial and noisy observations. This method is based on the assumption that the process under study, in this case the 3d wind, is Gaussian. Finally, as the 3d wind reconstructed using this method depends on the configuration of the lidar axes we will optimize these axes to minimize the standard deviation of the reconstruction error which is independent of the measurements.

In Section 2, we present the problem under study. Next, in Section 3, we introduce the von Karman model, which will serve as the physics-informed kernel in the Gaussian process regression method in Section 4. Finally, in Section 5, we will reconstruct the turbulent wind and optimize the lidar axes, assuming that the aircraft accumulates observations as it moves. We will see, both theoretically and numerically, that the oldest observations eventually cease to have any impact on the quality of the reconstruction.

## 2 Problem modeling

In this section, we review the problem under study as well as the notation as defined in Capmas-Pernet et al. (2026). Our objective is to determine the 3d wind $v(x^*)$ for a point of interest $x^*$ located upstream of the aircraft. To achieve this, the aircraft is equipped with a multi-axis UV lidar. Without going into too much detail about the physics involved, this is a system for determining the speed of molecules in the atmosphere. Thanks to it, it is possible to partially determine wind speed at several points on each axis. However, this is an optical system based on the Doppler effect, and it is therefore not possible to obtain, for a given measurement point, the 3d wind speed at that point, but only its projection on the target axis, in other words a scalar quantity.
Let $d$ be the number of axes and $\forall i \in [\![1,d]\!]$ let $a_i \in \mathbb{R}^3$ be a director vector of the $i$-th axis of the form (see Fig. 1):

$$a_i = \Big(\sin(\varphi_i)\sin(\theta_i), \sin(\varphi_i)\cos(\theta_i), \cos(\varphi_i)\Big)^T \quad (1)$$

with $\varphi_i$ and $\theta_i \in [0, 2\pi]$. On each axis we consider $n$ measurement points evenly distributed at distances, in meters, between $L_{min}$ and $L_{max}$. For the i-th axis, $\forall k \in [\![1,n]\!]$, these points are defined as follows:

$$x_{ki} = d_k a_i \text{ with } d_k = L_{min} + (k-1)\frac{L_{max} - L_{min}}{n-1} \quad (2)$$

At each point $x_{ki} \in \mathbb{R}^3$ is associated an observation $y_{ki} \in \mathbb{R}$ $(m/s)$ which is the projection of the 3d wind $v_{ki} \in \mathbb{R}^3$ at point $x_{ki}$ on axis $a_i$ plus an error term $\varepsilon_{ki}$ (in meters) which represents the error made when measuring the projected wind:

$$y_{ki} = {a_i}^T v_{ki} + \epsilon_{ki} \quad (3)$$

Here $v_{ki} = \big((v_{ki})_1, (v_{ki})_2, (v_{ki})_3\big)^T$ where $(v_{ki})_j = v_{ki}^T e_j$. The measurement noises are assumed to be independent and identically distributed samples from the distribution $\mathcal{N}(0, \sigma_{ins}^2)$ where $\sigma_{ins} \in \mathbb{R}_+$ is the measurement noise. We note $Y_{obs} \in \mathbb{R}^{nd}$ the vector containing all our observations, so that $(Y_{obs})_{(i-1)\times n+k} = y_{ki}$. In the same way, we stack all our 3d velocities into a vector $V \in \mathbb{R}^{3nd}$ :

$$V = \Big(v_{11}^T, \cdots, v_{n1}^T, v_{21}^T, \cdots, v_{nd}^T\Big)^T \quad (4)$$

Next we define the projection matrix $H \in \mathcal{M}_{nd,3nd}(\mathbb{R})$[1]

$$H = \begin{pmatrix} H_1 & 0 & \cdots & 0 \\ 0 & H_2 & \ddots & \vdots \\ \vdots & \ddots & \ddots & 0 \\ 0 & \cdots & 0 & H_d \end{pmatrix} \text{ with } H_i = I_n \otimes {a_i}^T \quad (5)$$

Our measures can therefore be rewritten as follows:

$$Y_{obs} = HV + \eta \quad (6)$$

With $\eta = (\epsilon_{11}, \cdots, \epsilon_{n1}, \epsilon_{12}, \cdots, \epsilon_{nd})^T$. Given $Y_{obs}$, our goal is to estimate the turbulent wind $v(x^*)$ as accurately as possible for a given point of interest $x^*$. To do this, we introduce a turbulent wind model that will be useful in the rest of the study

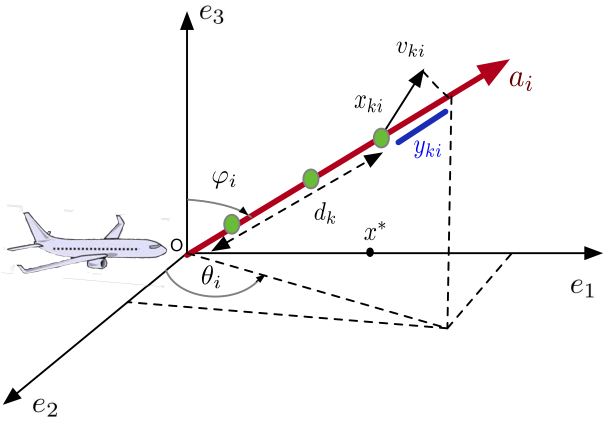


Figure 1: Partial observations on a lidar axis unit vector $a_i$ which is defined by the angles $\varphi_i$ and $\theta_i$. At point $x_{ki}$, at a distance $d_k$ on axis $a_i$, we measure the projection $y_{ki}$ of 3d wind $v_{ki}$ onto the lidar axis.

## 3 Modeling turbulence using the von Karman model

The von Karman model (von Kármán, 1948) is a model commonly used in aeronautics to model homogeneous and isotropic turbulent winds. This is a special case of the Reynolds-averaged Navier-Stokes equations applied to wind turbulence, where the time-averaged velocity is assumed to be zero. Its use is justified by experimental studies conducted on approximately homogeneous isotropic turbulence, such as the classic turbulence measurements performed by Comte-Bellot and Corrsin. These studies justify the use of second-order isotropic statistics and provide reference correlation functions (Comte-Bellot and Corrsin, 1971). The von Karman covariance is commonly used as an empirical parametric model for these second-order statistics, thereby allowing the behavior observed on large scales and in the inertial range to be reproduced, see F. dos Santos (2022). In particular, F. dos Santos (2022) notes that the Von Karman energy spectrum is one of the best-suited models for representing turbulence spectra in various applications. For two points $x$ and $y$, this model tells us that the covariance between the $i$-th component of $v(x)$ and the $j$-th component of $v(y)$ depends only on $r = x - y$ according to the formula (Batchelor, 1953; Pope, 2000, chapter 6):

$$\begin{aligned} R_{i,j}(r) &= \mathbb{E}[v_i(x)v_j(y)] \\ &= \sigma^2 \left[\frac{r_i r_j}{|r|^2}\big(f(|r|) - g(|r|)\big) + \delta_{ij} g(|r|)\right] \end{aligned} \quad (7)$$

with for the von Karman model (see Wilson, 1998, section 5):

- $r_i = x_i - y_i$ and $|r|$ the Euclidean norm of $r$

[1]the set of matrices with $nd$ rows and $3nd$ columns.

- $f(r) = \frac{2}{\Gamma(\frac{1}{3})}\left(\frac{r}{2l}\right)^{\frac{1}{3}} K_{\frac{1}{3}}\left(\frac{r}{l}\right)$
- $g(r) = \frac{2}{\Gamma(\frac{1}{3})}\left(\frac{r}{2l}\right)^{\frac{1}{3}} \left[K_{\frac{1}{3}}\left(\frac{r}{l}\right) - \frac{r}{2l}K_{\frac{2}{3}}\left(\frac{r}{l}\right)\right]$
- $K_\alpha(\cdot)$ modified Bessel function of the second kind of order $\alpha$ and $\delta_{ij}$ the Kronecker delta
- $\sigma \in \mathbb{R}_+$ characteristic intensity of turbulence $(m/s)$ and $l$ characteristic length scale of turbulence $(m)$

To simplify the notation, $\forall \mathbf{r} \in \mathbb{R}^3$ we note:

$$R(\mathbf{r}) \in \mathcal{M}_3(\mathbb{R}) \text{ s.t. } \big(R(\mathbf{r})\big)_{i,j} = R_{i,j}(\mathbf{r}) \tag{8}$$

This is the covariance matrix between the wind velocity vectors at two points separated by a vector $\mathbf{r}$. Finally, in a similar manner, it is possible to construct $\Sigma \in \mathcal{M}_{3nd}(\mathbb{R})$, the covariance matrix of the vector $V$ defined by Eq. (4).

$$\Sigma = (\Sigma_{i,j})_{1 \leq i,j \leq nd} \tag{9}$$

$$\Sigma_{(i-1)n+k,(j-1)n+l} = R(x_{ki} - x_{lj}) \in \mathcal{M}_3(\mathbb{R}) \tag{10}$$

This matrix will be used as a "physics-informed" kernel for wind reconstruction using a machine learning method called Gaussian process regression.

# 4 Gaussian process regression with physics-informed kernel

Gaussian process regression (also known as kriging, in reference to Krige, 1951) is a non-parametric machine learning method belonging to the class of kernel methods, which represents the output data of our model as realizations of a Gaussian stochastic process. In this section, we present a modified version of this method to adapt it to our case study. For the original version, see Rasmussen and Williams (2006).

## 4.1 General principle of the method

Assume that our 3d wind follows a centered Gaussian process with covariance/kernel $k : \mathbb{R}^3 \times \mathbb{R}^3 \to \mathcal{M}_3(\mathbb{R})$. More precisely, suppose that $V \sim \mathcal{N}(0, K)$ with $K = (K_{i,j})_{1 \leq i,j \leq nd}$ a block matrix with blocks of sizes $3 \times 3$ such that:

$$K_{(i-1)n+k,(j-1)n+l} = k(x_{ki}, x_{lj}) \in \mathcal{M}_3(\mathbb{R}) \tag{11}$$

In this case, according to Eq. (6), $Y_{obs}$ is a realization of the random vector $Y$ with distribution:

$$Y \sim \mathcal{N}\Big(0, HKH^T + \sigma_{ins}^2 I_d\Big) \tag{12}$$

Since wind is considered as a Gaussian process, for any point $z \in \mathbb{R}^3$, $v(z)$ is a Gaussian random variable. From observations $Y_{obs}$, we want to construct another random variable, $\hat{v}(x^*)$, which is as close as possible to the 3d wind at the point of interest $v(x^*)$ (for the distance induced by the inner product $(U, W) \mapsto \mathbb{E}[U^T W]$ for any two random vectors $U$ and $W$ with squared integrable Euclidean norm). The only random variable that minimizes this distance is the conditional expectation $\mathbb{E}[v(x^*)|Y]$, and our estimator of the reconstructed wind $\hat{v}(x^*)$ is defined by:

$$\hat{v}(x^*) = \mathbb{E}[v(x^*)|Y = Y_{obs}] \tag{13}$$

As we assume that $\begin{pmatrix} V \\ v(x^*) \end{pmatrix}$ is a centered Gaussian vector, and as the measurement noises are Gaussian, centered and independent, we have that $\begin{pmatrix} Y \\ v(x^*) \end{pmatrix}$ is a centered Gaussian vector with covariance:

$$\begin{pmatrix} HKH^T + \sigma_{ins}^2 I_d & H\mathrm{Cov}\big(v(x^*), V\big)^T \\ \mathrm{Cov}\big(v(x^*), V\big)H^T & k(x^*, x^*) \end{pmatrix} \tag{14}$$

with

$$\mathrm{Cov}\big(v(x^*), V\big) = \big(k(x^*, x_{11}) \cdots k(x^*, x_{nd})\big) \tag{15}$$

In the Gaussian case, the conditional expectation is calculated explicitly, and we have:

$$\hat{v}(x^*) = \mathrm{Cov}\big(v(x^*), V\big)H^T \left[HKH^T + \sigma_{ins}^2 I_d\right]^{-1} Y_{obs} \tag{16}$$

Furthermore, it can be shown that:

$$\mathbb{E}\left[\big(v(x^*) - \hat{v}(x^*)\big)\big(v(x^*) - \hat{v}(x^*)\big)^T\right] = \mathrm{Var}\big(v(x^*)|Y\big) \tag{17}$$

Again, the conditional covariance is calculated explicitly

$$\mathrm{Var}\big(v(x^*)|Y\big) = k(x^*, x^*) - \mathrm{Cov}\big(v(x^*), V\big)\cdot \\ H^T \left[HKH^T + \sigma_{ins}^2 I_d\right]^{-1} H\mathrm{Cov}\big(v(x^*), V\big)^T \tag{18}$$

This covariance matrix is independent of the observations and if we note by $\sigma_L^2, \sigma_T^2, \sigma_V^2$ the diagonal elements of this matrix, these three quantities can be interpreted respectively as the variances of the reconstruction errors in the longitudinal, transverse, and vertical components of velocity. Note that the reconstruction error is optimal only if the observations and the 3d wind at the point of interest define a Gaussian vector whose covariance matrix is known. In practice, this is not necessarily the case, since the covariance function $k$ is only an approximation of the true covariance.

## 4.2 Physics-informed kernel

The main drawback when using Gaussian process regression method lies in choosing a kernel function $k : \mathbb{R}^3 \times \mathbb{R}^3 \to \mathcal{M}_3(\mathbb{R})$ that is suitable for the problem. In general, classical kernel functions are chosen, such as Gaussian or Matérn kernels (see Genton, 2001, for more details), for which the hyperparameters are calibrated using a maximum likelihood method.
Here, we will choose a kernel function that takes advantage of the a priori knowledge of the physics of turbulence, based on the von Karman model to obtain what is known as a physics-informed kernel. In this case, the matrix $K$ corresponds to the matrix $\Sigma$ defined in Eq. (9). The von Karman model is an experimentally validated model, but it provides only the covariance

of our wind, not its distribution. The choice of the Gaussian model is motivated by the fact that it allows for optimal Bayesian inversion. We can see that this choice is robust even in the case of poor model specification. Indeed, if we generate our observations from a wind following a multivariate Student's distribution, we observe Table 1 that the empirical standard deviation, obtained with $10^5$ Monte Carlo simulations, of our reconstruction error on the vertical velocity is roughly equal to that obtained if the observations were from a Gaussian wind (i.e., when $\nu = +\infty$). Thus, although our model assumes a Gaussian prior, we observe that a distribution that differs significantly from the Gaussian (the Student's distribution being heavy-tailed) has no significant impact on the estimate.

Table 1: Empirical standard deviation of the reconstruction error in vertical velocity when the observations are derived from a wind generated by a centered multivariate Student's distribution with covariance $\Sigma$ and parameter $\nu$. Config 1 is the optimal configuration shown in Fig. 6(a). For Config 2, the four axes form a cone with a half-angle of $\pi/3$.

| | $\nu = 3$ | $\nu = 5$ | $\nu = 10$ | $\nu = +\infty$ |
|---|---|---|---|---|
| **Config 1** | 0.5893 | 0.5881 | 0.5877 | 0.5877 |
| **Config 2** | 0.6214 | 0.6256 | 0.6258 | 0.6260 |

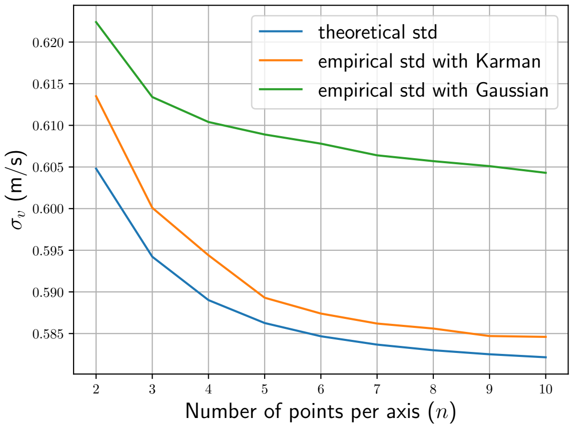


Figure 2: Standard deviation of the reconstruction error for vertical velocity as a function of the number of measurement points per axis. The red curve assumes that the turbulence parameters are known. The blue curve shows Monte Carlo standard deviations obtained by maximum likelihood estimates with the Von Karman kernel. The green curve represents the empirical standard deviation obtained using maximum likelihood estimation of the parameters of the Gaussian kernel $k(x, y) = \kappa^2 e^{-\lambda|x-y|^2} I_3$. For this figure, we use the same parameters as those in the scenario described in Section 5.3 with $m = 1$ and the optimal configuration shown in Fig. 6(a).

In practice, however, we do not have access to the true values of the turbulence parameters $\theta = (\sigma^2, l)$, Eq. (7), and they must be estimated using a maximum likelihood method.

Let $\Sigma_\theta$ denote the von Karman covariance matrix obtained by Eq. (9) with parameters $\theta = (\sigma^2, l)$. In this case, $(Y|\theta)$ follows a centered Gaussian distribution with covariance matrix:

$$C_\theta = H\Sigma_\theta H^T + \sigma_{ins}^2 I_d \tag{19}$$

We seek $\hat{\theta} = (\hat{\sigma}^2, \hat{l})$ that maximizes the (log-)likelihood of observing $Y_{obs}$:

$$\hat{\theta} = \arg\max_{\theta \in \mathbb{R}_+^2} -\frac{1}{2} \ln\left(|C_\theta|\right) - \frac{1}{2} Y_{obs}^T C_\theta^{-1} Y_{obs} \tag{20}$$

Remark that the gradient of this quantity can be calculated explicitly, thereby improving the convergence of the optimization.

Our estimator is then:

$$\hat{v}(x^*) = \mathrm{Cov}_{\hat{\theta}}(v(x^*), V) H^T C_{\hat{\theta}}^{-1} Y_{obs} \tag{21}$$

With this definition, the reconstructed wind is not exactly the conditional expectation given the observations. In fact, even if we assume a Gaussian wind with a covariance matrix given by the von Karman model, the turbulence parameters are approximated, and the covariance matrix in question is not the true one. Thus, it is possible that, on average, the quadratic reconstruction error obtained by maximum likelihood differs from the theoretically minimal error obtained given the true turbulence parameters. Nevertheless, for the method to be meaningful, this discrepancy must remain small.

To determine the extent to which the quality of our reconstruction deteriorates when the turbulence parameters are unknown we will estimate the reconstruction error obtained by maximum likelihood using a Monte Carlo method. We will focus only on the vertical component of the velocity because it is the component (with the transverse component) that will have the most significant impact on the aircraft, due to the aircraft's aerodynamics. The effect of longitudinal velocity is negligible compared to the aircraft's forward speed.

Let $N$ be the number of Monte Carlo simulations, $\forall i \in [\![1, N]\!]$ we generate observations $Y_{obs}^i$ and a wind $v^i(x^*)$ from Eq. (14) using the von Karman kernel, Eq. (8), with parameters $\sigma^2$ and $l$. Next, we estimate $\hat{\sigma}^i$ and $\hat{l}^i$ using maximum likelihood estimation. Then, using these parameters and Eq. (21), we obtain our reconstructed vertical wind $\hat{v}_3^i(x^*)$, which we compare with $v_3^i(x^*)$, the true vertical wind. The empirical standard deviation of our reconstruction error on vertical velocity is then:

$$\sqrt{\frac{1}{N}\sum_{i=1}^{N}\left(\hat{v}_3^i(x^*) - v_3^i(x^*)\right)^2} \tag{22}$$

Fig. 2 compares the empirical standard deviations obtained by maximum likelihood with the theoretical standard deviations obtained from the formula Eq. (18) for the true parameters $\sigma = 1m/s$ and $l = 750m$. Here, the estimates were obtained using $4 \times 10^5$ Monte Carlo iterations. Numerically, there is just a small difference between the two curves, obtained by increasing the number of measurement points per axis, which justifies the applicability of our method as well as its robustness. On average, the estimation of the parameter $\theta$ slightly affect the accuracy of the results. Finally, we compare these results with those obtained by using a Gaussian kernel for the reconstruction instead of the Von Karman kernel: $k(x, y) = \kappa^2 e^{-\lambda|x-y|^2} I_3$. In this case, the parameters $\kappa$ and $\lambda$ are estimated using maximum like-

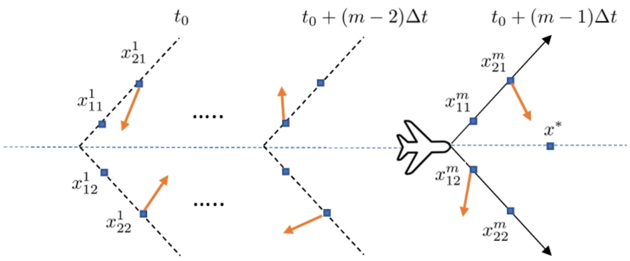


Figure 3: Illustration of the aircraft's motion. At time $t_0 + (m-1)\Delta t$, measurements are taken at points $x_{ki}^m$

lihood. The empirical standard deviations are consistently lower than those obtained with the Von Karman kernel. These differences stem from the fact that the reconstruction model does not match the model from which the wind is derived.

# 5 Accounting for the aircraft's movement

Until now, we have considered observations in a static setting, however, to improve the results, we will want to take advantage of the observations made by the aircraft as it moves.

## 5.1 Reconstruction with forward movement of the aircraft

At a given time $t_0$, we have $n \times d$ partial/projected measurements of the turbulent wind. However, our aircraft is in motion and, after a time interval $\Delta t$, it will have moved a distance $\Delta x$ along the $x$-axis Fig. 1. Thus, if at time $t_0$ the measurements are taken at the points $\{x_{11}, \cdots, x_{nd}\}$ defined in Eq. (2), then after a time $(m-1) \times \Delta t$ the measurements will be taken at the points (see Fig. 3):

$$(x_{ki}^m)_{1\leq k\leq n}^{1\leq i\leq d} \quad \text{where} \quad x_{ki}^m = x_{ki} + (m-1)\Delta x \begin{pmatrix}1\\0\\0\end{pmatrix} \tag{23}$$

At time $t_{m-1} = t_0 + (m-1)\Delta t$ we have $n \times d \times m$ observations from which we want to reconstruct the wind at the point:

$$x_m^* = x^* + (m-1)\Delta x \begin{pmatrix}1\\0\\0\end{pmatrix} \tag{24}$$

where the origin of the coordinate system is taken to be the aircraft's position at time $t_0$.

Let $\hat{v}_m(x^*)$ denote the wind vector reconstructed from these $n \times d \times m$ observations in order to approximate $v(x_m^*)$ at time $t_{m-1}$. Similarly to Eq. (16), our estimator is defined as follows:

$$\hat{v}_m(x^*) = \mathrm{Cov}\big(v(x_m^*), V\big) H^T \left[H\Sigma H^T + \sigma_{ins}^2 I_d\right]^{-1} Y_{obs} \tag{25}$$

The difference lies in the expressions of the matrices $H$, $V$, $\Sigma$, and $Y_{obs}$, which take into account our $n \times d \times m$ measurement points. So $H \in \mathcal{M}_{ndm,3ndm}(\mathbb{R})$, $V$ and $\Sigma \in \mathcal{M}_{3ndm,3ndm}(\mathbb{R})$ et $Y_{obs} \in \mathbb{R}^{ndm}$.

Finally, for the von Karman kernel, Eq. (18), the covariance matrix of the reconstruction error is:

$$\begin{aligned}\mathrm{Var}\big(v(x_m^*)|Y\big) = \sigma^2 I_3 - \mathrm{Cov}\big(v(x_m^*), V\big)\cdot \\ H^T \left[H\Sigma H^T + \sigma_{ins}^2 I_d\right]^{-1} H \mathrm{Cov}\big(v(x_m^*), V\big)^T\end{aligned} \tag{26}$$

By increasing the number of observations, we expect to obtain a more accurate reconstruction of the wind. However, as the number of observations increases, the matrices involved become larger, which can lead to numerical errors during matrix inversion in Eq. (25). Furthermore, as $m$ increases, the distances between the first and last measurement points grow larger, resulting in a decorrelation between the wind speeds at the observation points. To observe this phenomenon, let us perform an asymptotic limited expansion of our reconstruction error in a simple case when the distance between the point of interest and the aircraft tends to infinity.

## 5.2 Asymptotic decorrelation

Suppose we have only one measurement $x_1$ located at a distance $d$ along a normed axis $a = (a_1, a_2, a_3)^T$, such that $x_1 = da$. The point of interest is at a distance $r$ along the axis of the plane: $x^* = (r, 0, 0)^T$. In this simplified case, $(H\Sigma H^T + \sigma_{ins}^2)^{-1} = \frac{1}{\sigma^2+\sigma_{ins}^2}$ and the standard deviation of our reconstruction error for vertical velocity ($\sigma_V$) is given by:

$$\sigma_V = \sqrt{\sigma^2 - \frac{1}{\sigma^2 + \sigma_{ins}^2}\Big(cov\big(v_3(x^*), a^T v(x_1)\big)\Big)^2} \tag{27}$$

We wish to determine the asymptotic rate of convergence of the quantity $\sigma_V$ as $r \to +\infty$.

To simplify the notation, we note:

$$A(r) \stackrel{\text{def}}{=} \frac{1}{\sigma^2} cov\big(v_3(x^*), a^T v(x_1)\big) \tag{28}$$

Hence,

$$\sigma_V \underset{+\infty}{\sim} \sigma - \frac{1}{2} \times \frac{\sigma^2}{\sigma^2 + \sigma_{ins}^2} A(r)^2 \tag{29}$$

By taking,

- $p(r) = -rda_1a_3 + d^2a_3$
- $q(r) = \|x^* - x_1\|^2 = r^2 + d^2 - 2rda_1$

We get,

$$A(r) = \frac{p(r)}{q(r)}\left[f\left(\sqrt{q(r)}\right) - g\left(\sqrt{q(r)}\right)\right] + a_3 g\left(\sqrt{q(r)}\right) \tag{30}$$

After expanding the calculations, we obtain:

$$\begin{aligned}A(r) = \frac{2}{\Gamma\left(\frac{1}{3}\right)}\left(\frac{\sqrt{q(r)}}{2L_0}\right)^{1/3}\Bigg[K_{\frac{2}{3}}\left(\frac{\sqrt{q(r)}}{L_0}\right) \times \frac{\sqrt{q(r)}}{2L_0} \\ \times \left(\frac{p(r)}{q(r)} - a_3\right) + K_{\frac{1}{3}}\left(\frac{\sqrt{q(r)}}{L_0}\right) \times a_3\Bigg]\end{aligned} \tag{31}$$

According to Abramowitz and Stegun (1964) , $\forall \nu \in \mathbb{C}$, in the first order, we have:

$$K_\nu(r) \underset{+\infty}{\sim} \sqrt{\frac{\pi}{2r}} e^{-r} \tag{32}$$

In particular $K_{1/3}(r) \underset{+\infty}{\sim} K_{2/3}(r)$ and after some calculations, we get:

$$A(r) \underset{+\infty}{\sim} -\frac{a_3\sqrt{\pi}}{\Gamma\left(\frac{1}{3}\right)} \left(\frac{r}{2l}\right)^{5/6} e^{-\frac{r-da_1}{l}} \tag{33}$$

Finally, as $A(r) \to 0$ when $r \to +\infty$,

$$\sigma_V \underset{+\infty}{\sim} \sigma - \frac{\sigma^2}{\sigma^2+\sigma_{ins}^2} \times \frac{a_3^2\pi}{2\Gamma\left(\frac{1}{3}\right)^2} \left(\frac{r}{2l}\right)^{5/3} e^{-\frac{2}{l}(r-da_1)} \tag{34}$$

From this equation, we can determine the optimal axis when the point of interest is at infinity. Indeed, this optimal axis lies in the plane $(e_1, e_3)$, and we simply need to find $a_1 \in [-1, 1]$ that minimizes Eq. (34) with $a_3^2 = 1 - a_1^2$. The solution is given by:

$$a_1 = \left(-1 + \sqrt{1 + \left(\frac{2d}{l}\right)^2}\right) \times \frac{l}{2d} \tag{35}$$

With angular notations (Eq. (1), Fig. 1), the optimal axis is parametrized by the angles:

$$\begin{cases} \theta = \dfrac{\pi}{2} \\ \varphi = \sin^{-1}\left(-\dfrac{l}{2d} + \sqrt{1 + \left(\dfrac{l}{2d}\right)^2}\right) \end{cases} \tag{36}$$

We observe that this axis does not coincide with the axis of displacement of the aircraft to which the point of interest $x^*$ belongs. In particular, the closer the measurement point is, the more the optimal axis tends to be vertical. However, the information provided by the measurement at $x_1$ is negligible. Indeed, from Eq. (34), we know that asymptotically, the standard deviation of the reconstruction error in the vertical velocity ($\sigma_V$) converges to the characteristic turbulence intensity ($\sigma$) with a convergence rate given in $\mathcal{O}\left(r^{5/3}e^{-2r/l}\right)$.

In Fig. 4, we can see this asymptotic convergence . We start with an axis $a$ parameterized as in Eq. (1) with $\theta = \pi/3$ and $\varphi = \pi/4$; the measurement point is located at a distance $d = 100m$. Graphically, we observe that when the measurement point is approximately $1000m$ away from the point of interest, the standard deviation of the reconstruction error is equivalent to the standard deviation of the wind without prior information. The winds at these two points are completely uncorrelated, and the observation at $x_1$ provides no information about the wind at $x^*$. It is therefore not necessary to accumulate observations, as the oldest ones eventually cease to provide any information about the wind we are trying to reconstruct.

## 5.3 Angle optimization

If we look closely at the equations Eq. (25) and Eq. (26), which give the reconstructed 3d wind and the variance

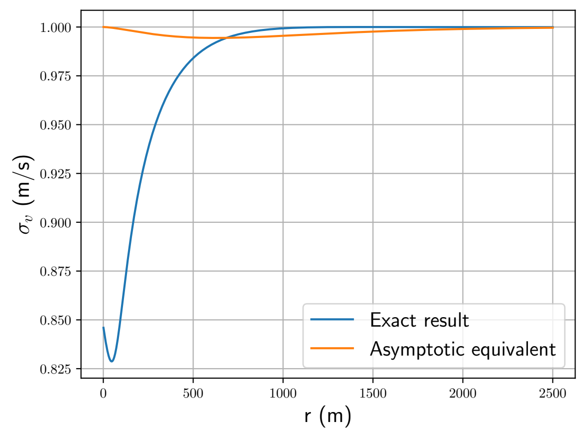


Figure 4: Standard deviation of the reconstruction error in vertical velocity as a function of distance from the point of interest. The blue curve represents the true standard deviation, and the red curve represents its asymptotic equivalent. Here $\sigma = 1m/s$, $\sigma_{ins} = 0.1m/s$ and $a$ is defined by Eq. (1) with $\theta = \pi/3$ and $\varphi = \pi/4$.

of our reconstruction error, respectively, we can see that they depend only on our lidar axes. This is obvious from the fact that they depend on the matrix $H$, which is the projection matrix onto the axes.

We will therefore seek a configuration $\Theta = (\theta_i, \varphi_i)_{1\leq i\leq d} \in [0, 2\pi]^{2d}$ on our axes $(a_i)_{1\leq i\leq d}$ Eq. (1) that minimizes our reconstruction error. The result will depend on which criterion we choose to optimize. The main criterion we will consider is the standard deviation of the reconstruction error on the vertical component of velocity (criterion $C_1$), as this is the one that will have the greatest impact on the aircraft. However, we can also consider the error in the transverse component in addition to that in the vertical component (criterion $C_2$)

$$\begin{cases} C_1(\Theta) = \sigma_V(\Theta) \\ C_2(\Theta) = \dfrac{1}{\sqrt{2}}\sqrt{\sigma_T^2(\Theta) + \sigma_V^2(\Theta)} \end{cases} \tag{37}$$

where $\sigma_V$ and $\sigma_T$ are defined by Eq. (18). To numerically study the optimal reconstruction error, we will consider a scenario with the following parameters:

- Turbulence intensity: $\sigma = 1m/s$
- Characteristic length scale of turbulence: $l = 750m$
- Instrumental noise : $\sigma_{ins} = 0.1m/s$
- $L_{min} = 100m$, $L_{max} = 300m$
- $n = 4$, $d = 4$ and $m \in [\![1, 20]\!]$
- $\Delta t = 0.1s$ and $\Delta x = 20m \implies$ speed of $720km/h$
- Point of interest at $100m$ from the aircraft

The optimal angles are obtained through numerical optimization, in this case using the BFGS method. To avoid converging to a local minimum, the algorithm is run multiple times, each time starting from a random point selected from $[0, 2\pi]^{2d}$, and only the best result is retained. In practice, the computation time required to

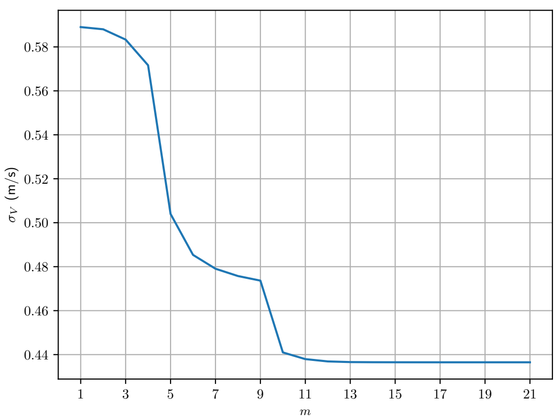


Figure 5: Standard deviation of the reconstruction error in vertical velocity as a function of the number of time steps $m$ for the cumulative observations. For each $m$, the result is obtained using an optimal axis configuration. The parameters considered are those defined in 5.3.

obtain an optimal configuration is not a limiting factor. Indeed, once the arrangement of the lidar axes on the aircraft is chosen, it is final; thus, the optimization is not a procedure to be performed during flight, unlike the reconstruction method, which must be applied in real time. Fig. 5 shows the standard deviation of the reconstruction error in vertical velocity as a function of the number of time steps $m$ for the cumulative observations. For each $m$, we seek the configuration $\Theta_m^*(x^*)$ that minimizes $C_1(\Theta)$, and it is this optimal standard deviation that is plotted on the $y$-axis. In other words, the orientation of the axes varies along this curve.

When we increase the number of time steps $m$ for aggregating observations, we would logically expect our reconstructed wind to be more accurate. However, we saw earlier that once measurement points are too far from the point of interest, they no longer provide any useful information, according to Eq. (34) and Fig. 4. With $\Delta x = 20m$, we therefore expect that beyond $m = 50$, the oldest observations will have no impact. In reality, as can be seen in Fig. 5, this phenomenon occurs much earlier. For our scenario, this occurs around $m = 10$. This can be explained by the fact that when $m = 10$, the closest observations are located approximately $100m$ from the aircraft's position at time $t_0$, and the farthest ones at a distance of $500m$. The point of interest, meanwhile, is located at a distance of $300m$ (relatively to the aircraft's position at time $t_0$). In other words, the measurement points encompass the point of interest, and the information obtained from observations at more distant points is largely contained within these points. Fig. 6 shows the optimal axes for criteria $C_1$ and $C_2$ when $m = 1$ and $m = 10$. First observation, no axis is parallel to the aircraft's axis. Indeed, with such an axis, we would be as close as possible to the point of interest, but at the same time the projection of the vertical and transverse components of the velocity onto this axis would be zero, which would provide no information. In the case of criterion $C_1$, all four axes lie in the $(e_1, e_3)$ plane, which is consistent with the fact that we only wish to reconstruct the vertical velocity.

For criterion $C_2$, the axes are no longer in the same plane, since we are also seeking to accurately estimate the transverse velocity, and for optimal axes we obtain $\sigma_T = \sigma_V$. In any case, we consistently observe a 2-by-2 symmetric arrangement of our axes relatively to the aircraft's axis, see Table 2. This is a consequence of the isotropy property of the turbulence derived from the von Karman model. Finally, it should be noted that taking cumulative observations into account significantly reduces the standard deviation of the reconstruction error (by about 40%). Furthermore, our estimator requires only matrix products and inversions to be computed. Its algorithmic complexity is $\mathcal{O}\big((ndm)^3\big)$. In our scenario, where $n = 4$, $d = 4$, and $m = 10$ is sufficient, this poses no problem for real-time computations.

Table 2: Angles (in degrees) between the aircraft's axis and each of the 4 lidar axes. The lidar axes considered are the optimal axes for criteria $C_1$ and $C_2$ with $m = 1$ and $m = 10$.

| | | Axis 1 | Axis 2 | Axis 3 | Axis 4 |
|---|---|---|---|---|---|
| $C_1$ | $m = 1$ | 37.64 | 56.88 | 37.64 | 56.88 |
| | $m = 10$ | 35.32 | 43.41 | 43.41 | 35.32 |
| $C_2$ | $m = 1$ | 48.98 | 48.98 | 48.98 | 48.98 |
| | $m = 10$ | 31.90 | 31.90 | 36.18 | 36.18 |

# 6 Conclusion

We have developed a method for reconstructing 3d turbulent wind from partial and noisy observations that can take into account measurements accumulated over time. The proposed method is optimal in the sense that it is the only function of the observations that minimizes the mean squared error. This method, known as Gaussian process regression, relies on an appropriate choice of the covariance function for our observations. The 3d turbulent wind is thus viewed as a stochastic process whose covariance/kernel function is given by the von Karman turbulence model. This model is used as a "physics-informed kernel" in Gaussian process regression to take advantage of prior knowledge of the turbulence structure. The reconstruction method is robust; on average, an error in the estimate of the turbulence parameters slightly affects the reconstruction error. Since the reconstructed wind field depends on the lidar angles, these angles are optimized to minimize the standard deviation of the reconstruction error. This optimization can be performed after taking into account that the aircraft accumulates observations as it moves, thereby improving the quality of the reconstruction. Numerically, for an aircraft traveling at $700km/h$, 10 sets of measurements are sufficient, and an improvement in accuracy of approximately 40% is observed compared to the static case. Finally, it may be interesting to generalize our reconstruction method to non-homogeneous and non-isotropic turbulence.

## References


M. Abramowitz and I. A. Stegun. *Handbook of Mathematical Functions with Formulas, Graphs, and Math-*

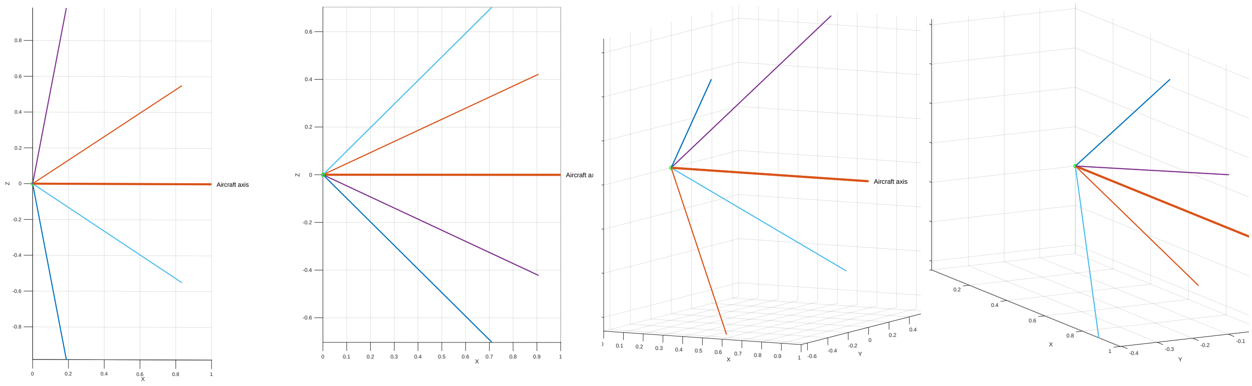


(a) (b) (c) (d)

Figure 6: Optimal axes for criterion $C_1$ with (a) $m = 1$ and (b) $m = 10$, and optimal axes for criterion $C_2$ with (c) $m = 1$ and (d) $m = 10$. We consider the parameters defined in section 5.3. For criterion $C_1$, the axes all lie in the same plane. For criterion $C_2$ with $m = 1$, they form a cone with a half-angle of 48.98°. When $m = 10$, they are symmetric in pairs with respect to a plane passing through the axis of the plane.


*ematical Tables*. Dover, New York, ninth dover printing, tenth gpo printing edition, 1964.

G. K. Batchelor. *The theory of homogeneous turbulence*. Cambridge monographs on mechanics and applied mathematics 810691884. Cambridge University Press, London [etc, 1953.

A. Capmas-Pernet, C. Musso, F. Dambreville, M. Valla, and T. Michel. Physics-informed machine learning for reconstruction of wind turbulence with wind lidar. *In: Machine Learning, Optimization, and Data Science, LOD 2025. Lecture Notes in Computer Science, volume 16467, to be published*, 2026.

G. Comte-Bellot and S. Corrsin. Simple eulerian time correlation of full-and narrow-band velocity signals in grid-generated, 'isotropic' turbulence. *Journal of Fluid Mechanics*, 48(2):273–337, 1971. doi: 10.1017/S0022112071001599.

C. V. F. dos Santos, Laura Botero-Bolívar. Modeling the turbulence spectrum dissipation range for leading-edge noise prediction. *AIAA Journal*, 2022.

N. Fezans, H.-D. Joos, and C. Deiler. Gust load alleviation for a long-range aircraft with and without anticipation. *CEAS Aeronautical Journal*, 10: 1033–1057, 2019. URL https://doi.org/10.1007/s13272-019-00362-9.

M. G. Genton. Classes of kernels for machine learning: a statistics perspective. *Journal of machine learning research*, 2(Dec):299–312, 2001.

D. Krige. A statistical approach to some basic mine valuation problems on the witwatersrand. *Journal of the Southern African Institute of Mining and Metallurgy*, 52(6):119–139, 1951. doi: 10.10520/AJA0038223X_4792. URL https://journals.co.za/doi/abs/10.10520/AJA0038223X_4792.

V. Y. Krishnamurthy. Formalization of flight mechanical cs-25 requirements for assessments using flight simulation in preliminary aircraft design. 2023. URL https://api-depositonce.tu-berlin.de/server/api/core/bitstreams/8e8d9e81-d0d4-49ca-9834-a79f4f2d747c/content.

C. Musso, T. Boulant, M. Valla, S. Lefebvre, and D. T. Michel. Estimation of the parameters of a three-dimensional gust model with a wind lidar. *AIAA Journal*, pages 1–12, 2024.

S. B. Pope. *Turbulent Flows*. Cambridge University Press, 2000.

C. E. Rasmussen and C. K. I. Williams. *Gaussian Processes for Machine Learning*. The MIT Press, 2006.

T. von Kármán. Progress in the statistical theory of turbulence. *Proceedings of the National Academy of Sciences*, 34(11):530–539, 1948. doi: 10.1073/pnas.34.11.530. URL https://www.pnas.org/doi/abs/10.1073/pnas.34.11.530.

D. K. Wilson. Turbulence models and the synthesis of random fields fo acoustic wave propagation calculations. Technical Report ARL-TR-1677, Army Research Laboratory, 1998.